Polymer 51 (2010) 5695–5704

Contents lists available at ScienceDirect

Polymer

journal homepage: www.elsevier.com/locate/polymer

Control of peptide secondary structure on star shape polypeptides tethered to polyhedral oligomeric silsesquioxane nanoparticle through click chemistry

Shiao-Wei Kuo*, Hsin-Tung Tsai

Department of Materials and Optoelectronic Science, Center for Nanoscience and Nanotechnology, National Sun Yat-Sen University, Kaohsiung, Taiwan

ARTICLE INFO

Article history:
Received 27 July 2010
Received in revised form
29 September 2010
Accepted 2 October 2010
Available online 12 October 2010

Keywords:
POSS
Nanocomposites
Polypeptide

ABSTRACT

New macromolecular self-assembling building blocks, star polypeptide-*b*-polyhedral oligomeric silsesquioxane (POSS) copolymers, were synthesized from octa-azido functionalized POSS ($OVBN_3$-POSS) with alkyne-poly(γ-benzyl-L-glutamate) (alkyne-PBLG) via a click reaction. The incorporation of POSS units at the core of PBLG moieties plays an important role, allowing intramolecular hydrogen bonding between the POSS and PBLG units to enhance the α-helical conformations in the solid state based on Fourier Transform Infrared spectroscopy (FTIR), solid state nuclear magnetic resonance (NMR), and wide-angle X-ray diffraction (WAXD) analyses.

1. Introduction

Polypeptides are polymers of receiving much interest because of their close relationship to proteins, their flexibility in functionality, and their molecular recognition properties. It is well known that the secondary structure of peptide chains plays a crucial role in the formation of the well-defined tertiary structure of proteins [1]. Poly(γ-benzyl-L-glutamate) (PBLG) is a synthetic polypeptide, it forms hierarchically order structure containing α-helix, which can be regarded as a rigid rod stabilized by intramolecular hydrogen bonding interaction and β-sheet secondary structures stabilized by intermolecular interaction as a fundamental secondary motifs [2]. The α-helical structure of PBLG serves as a rigid rod like structure in solid and solution state [3], which provides its unique bulk and solution behavior such as thermotropic liquid crystalline ordering [4,5] and thermo-reversible gelation, respectively [6,7].

Conformational studies of model polypeptides are an important step toward mimicking the biological activity of more complex proteins [8]. Therefore, rod–coil block copolymers based on a rigid PBLG helix have been studied extensively for several decades that follow nature's strategies for producing supramolecular bioactive assemblies with potential application is tissue engineering and drug delivery [9–19]. In our previous study [20], we combined the well-defined macromolecular architectures of polyhedral oligomeric silsesquioxane (POSS) and PBLG to generate polymeric building blocks having distinct 3-D shapes for the self-assembly of supramolecular structures through the ring-opening polymerization (ROP) of γ-benzyl-L-glutamate *N*-carboxyanhydride (γ-Bn-Glu NCA) using aminopropyl isobutyl-POSS as a macroinitiator. POSS derivatives comprise a family of molecularly precise, near-isotropic molecules that have diameters ranging from 1 to 3 nm, depending on the number of silicon atoms in the central cage and the nature of its peripheral substituent groups [21–29]. Two well-defined macromolecular architectures, POSS and PBLG, could be combined to generate polymer building blocks with well-defined 3-D shapes, which dictate the self-assembly process and resulting in supramolecular structures. Because of their unique structures, POSS derivatives are useful building blocks for the preparation of nanostructured materials. The POSS moiety incorporated at the chain end of the PBLG unit plays two important roles: (a) allowing intramolecular hydrogen bonding to occur between the POSS and PBLG units to enhance the latter's α-helical conformations in the solid state and (b) preventing the aggregation of nanoribbons although the POSS blocks' protrusion from the ribbons results in the formation of clear gels in solution. However, the PBLG-*b*-POSS in this case is prepared through the so-called divergence or graft from method, it is difficult to distinguish how the POSS nanoparticle to influence the secondary structure of PBLG. In this study, we use the convergence or coupling method to synthesize the star PBLG-*b*-POSS copolymers through click chemistry. Polymer architecture is

* Corresponding author. Tel./fax: +886 7 5254099.
E-mail address: kuosw@faculty.nsysu.edu.tw (S.-W. Kuo).

0032-3861/$ – see front matter © 2010 Elsevier Ltd. All rights reserved.
doi:10.1016/j.polymer.2010.10.005

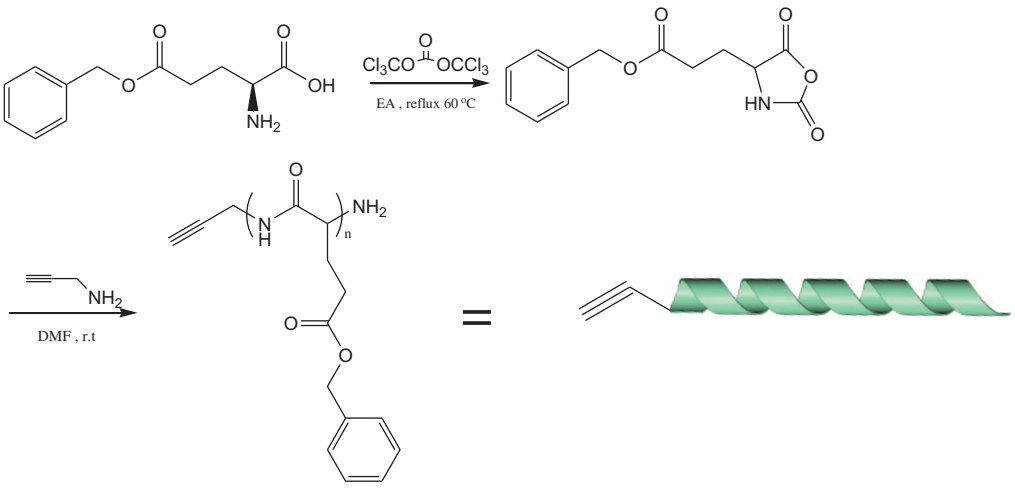

Scheme 1. The synthesis of alkyne-PBLG.

one of several factors that affect the self-assembly of block copolymers [9,30,31] The PBLG could adopt different secondary structure from their linear analogues. In the first place, we synthesize the different degree of polymerizations of alkyne-PBLG through ring-opening polymerization (ROP) of γ-benzyl-L-glutamate *N*-carboxyanhydride using propargylamine as a macroinitiator as shown in Scheme 1. Secondly, the star PBLG-*b*-POSS copolymers were synthesized from octa-azido functionalized POSS (OVBN$_3$-POSS) with alkyne-PBLG via a click reaction as shown in Scheme 2. The secondary structures of PBLG are characterized by Fourier Transform Infrared spectroscopy (FTIR), solid state nuclear magnetic resonance (NMR), and wide-angle X-ray diffraction (WAXD) analyses in this study.

2. Experimental

2.1. Materials

Propargylamine were purchased from Tokyo Kasei Kogyo Co., Japan. Vinyl benzyl chloride (VBC), *N*,*N*-dimethylformamide,sodium azide (NaN_3), copper(I) bromide (CuBr, 98%), *N*,*N*,*N*′,*N*″,*N*″-penta methyldiethylenetriamine (PMDETA, 99%), and platinum complex (platinum-1,3-divinyltetramethyldisiloxane, Pt-dvs, 2 wt% Pt in xylene) were purchased from Aldrich, USA. Before use, the solution of the platinum complex was diluted 100-fold with xylene. Toluene was dried by distillation before use in the hydrosilylation reaction. Octakis(dimethylsiloxy)silsesquioxane ($Q_8M_8^H$) containing

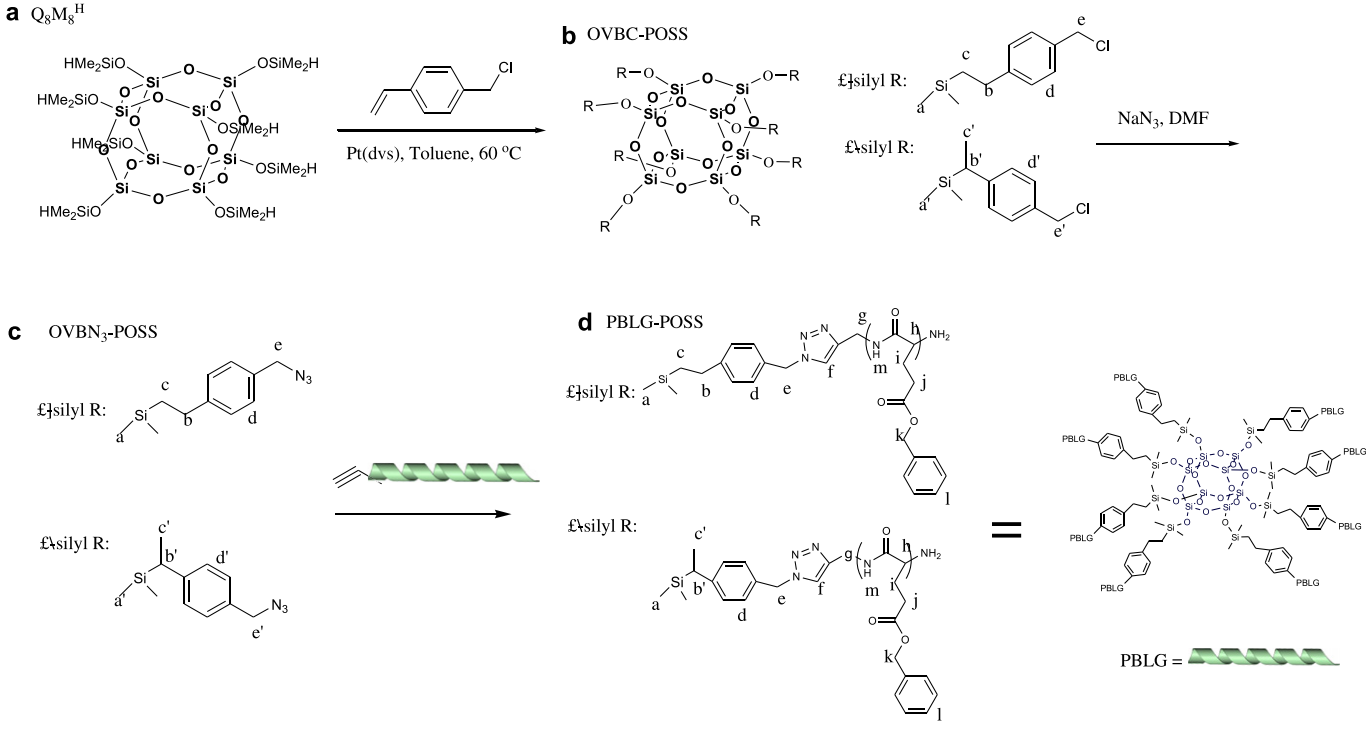

Scheme 2. The synthesis of star PBLG-*b*-POSS.

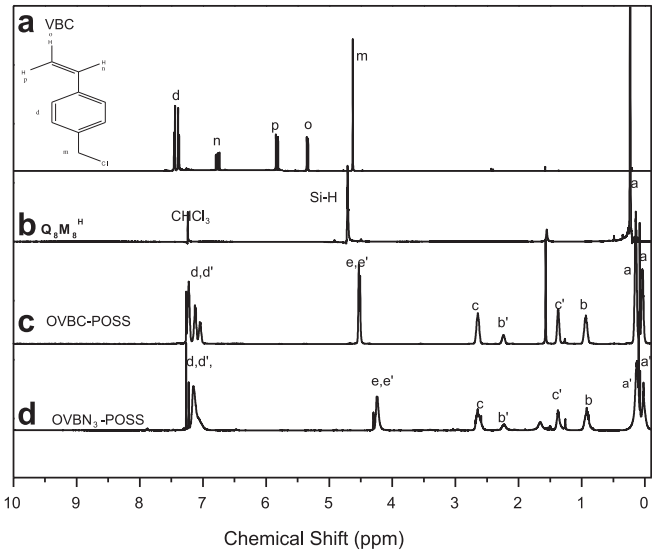

Fig. 1. ^{1}H NMR of (a) VBC, (b) Q8M8H, (c) OVBC-POSS, and (d) $OVBN_3$-POSS in $CDCl_3$.

eight hydro-silane groups was purchased from the Hybrid Plastics Co., USA. γ-Benzyl-L-glutamate *N*-carboxyanhydride was prepared according to a literature procedure [32] and stored at −30 °C.

2.2. Synthesis of $OVBN_3$-POSS

$OVBN_3$-POSS was synthesized via the reaction between OVBC-POSS and sodium azide (NaN_3) as shown in Scheme 1 [33]. The OVBC-POSS was prepared via $Q_8M_8^H$ (1 g, 0.98 mmol) and vinyl benzyl chloride (1.20 g, 7.86 mmol) in toluene (50 mL). The solution was heated at 60 °C under argon and Pt(dvs) (0.07 mL, 0.13 mmol) was added via syringe. After stirring for 4 h, removal of the Pt(dvs) catalyst was through activated charcoal. The solvent in a rotary evaporator gave a viscous liquid. We use the ^{29}Si NMR to determine the chemical structure OVBC-POSS. The ^{29}Si NMR of $Q_8M_8^H$ has two peaks at $(CH_3)_2\underline{\mathbf{Si}}$–H: −2.1 ppm and $\underline{\mathbf{Si}}$–O–Si $(CH_3)_2$H: 109.3 ppm. In addition, the ^{29}Si NMR of OVBC-POSS has three peaks at 10.28 ppm for $(CH_3)_2\underline{\mathbf{Si}}$-$(CHCH_3)$ and 12.16 ppm for $(CH_3)_2\underline{\mathbf{Si}}$–$CH_2$–$CH_2$– and −109.2 ppm for $\underline{\mathbf{Si}}$–O–$Si(CH_3)_2$H. Clearly, the chemical shift indicates that the hydrosilylation reaction occurred to completion under the reaction conditions.

Table 1
Molecular characteristics of the alkyne-PBLG.

Compound	Mn	DP	First-order transition
$PBLG_4$	929	4	–
$PBLG_6$	1367	6	106.0
$PBLG_{14}$	3119	14	108.6
$PBLG_{26}$	5747	26	115.2
$PBLG_{53}$	11660	53	116.0

In a typical experiment of synthesizing $OVBN_3$-POSS, OVBC-POSS (1 g, 0.45 mmol), NaN_3 (1.01 g, 15.4 mmol) and anhydrous DMF (50 mL) were added to a flask. The reaction was thermo stated at 120 °C for 48 h. The solvents were concentrated and the residues were dissolved in THF removal of the sodium salts through a neutral alumina column. The yellowish viscous liquid was obtained after drying in a vacuum oven overnight at room temperature.

2.3. Synthesis of alkyne-PBLG [34]

In a typical experiment for synthesizing alkyne-PBLG (Bn-Glu NCA), (4 g, 15.2 mmol) was weighed in a glovebox under pure argon, introduced in a flame-dried Schlenk, and dissolved with 40 mL of anhydrous DMF. The solution was stirred for 10 min, and propargylamine (12 μL, 175.2 μmol) was added with a nitrogen purged syringe. The solution was stirred for 40 h at room temperature. The polymer was recovered by precipitation in diethylether and dried under high vacuum.

2.4. Synthesis of star PBLG-b-POSS copolymers

$OVBN_3$-POSS (0.0115 g), alkyne-PBLG (0.5 g) and CuBr (3.5 mg, 0.025 mmol) were dissolved in DMF (20 mL) in a flask equipped

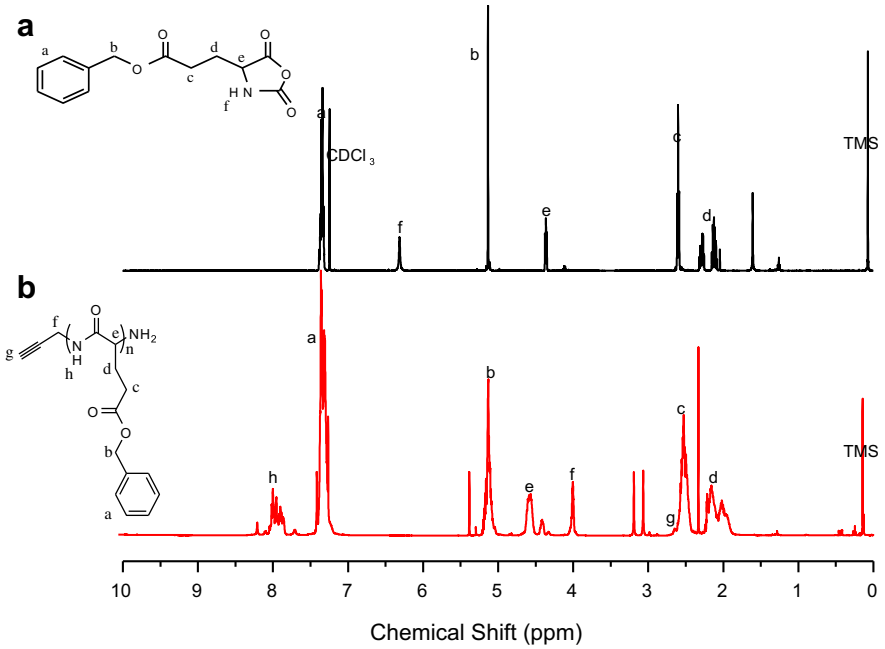

Fig. 2. ^{1}H NMR of (a) BLG monomer in $CDCl_3$, (b) alkyne-PBLG in $CDCl_3$ + 15 wt% TFA.

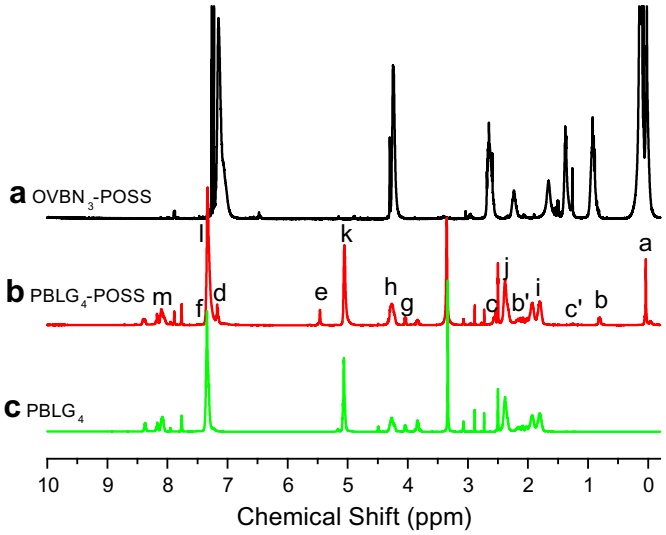

Fig. 3. ^{1}H NMR of (a) OVBN$_3$-POSS in CDCl$_3$, (b) star PBLG$_4$-*b*-POSS and (c) PBLG$_4$ in d-DMSO.

with magnetic stirring bar. After one brief freeze-thaw-pump cycle, PMDETA (5.2 μL, 0.025 mmol) was added and the reaction mixture was carefully degassed by three freeze-thaw pump cycles, placed in an oil bath thermostated at 60 °C and stirred for 24 h. After removing all the solvents at reduced pressure, the residues were dissolved in CH_2Cl_2 and passed through a neutral alumina column to remove copper catalysts. A dark powder of star PBLG-*b*-POSS was obtained.

2.5. Characterization

^{1}H and ^{13}C NMR spectra were recorded at room temperature on a Bruker AM 500 (500 MHz) Spectrometer using the residual proton resonance of the deuterated solvent as the internal standard. High-resolution solid-state ^{13}C NMR experiments were carried out at room temperature using a Bruker DSX-400 Spectrometer operating at resonance frequencies of 399.53 and 100.47 MHz for ^{1}H and ^{13}C, respectively. Thermal analysis through differential scanning calorimetry (DSC) was performed using a DuPont 910 DSC-9000 controller at a scan rate of 10 °C/min over a temperature range from 25 to 120 °C under a nitrogen atmosphere. FTIR spectra of the polymer films were recorded using the conventional KBr disk method. The films used in this study were sufficiently thin to obey the Beer–Lambert law. FTIR spectra were recorded using a Bruker Tensor 27 FTIR spectrophotometer; 32 scans were collected at a spectral resolution of 1 cm^{-1}. Because polymers containing hydroxyl groups are hygroscopic, pure N_2 gas was used to purge the spectrometer's optical box to maintain sample films dried. X-ray diffraction data were collected on the wiggler beamline BL17A1 of the NSRRC, Taiwan. A triangular bent Si (111) single crystal was employed to obtain a monochromated beam of wavelength $\lambda = 1.3344$ Å. The XRD patterns were collected using imaging plate (IP; Fuji BAS III, area = 20 × 40 cm^2) curved with a radius equivalent to the sample-to-detector distance of 280 mm. With 100 μm pixel resolution of the IP and a typical exposure time of 15 min, the XRD was measured cover a range of values of Q from 0.05 to 2.2 Å^{-1}, where the X-ray vector transfer $Q = 4\pi \sin(\theta)/\lambda$ is defined by the scattering angle 2θ and λ. The two-dimensional X-ray diffraction patterns observed for the sample (typical diameter 10 mm; thickness 1 mm) were circularly averaged to one-dimensional diffraction profile $I(Q)$, with Q value calibrated using standard samples of Ag-Behenate and Si powder (NBS 640b).

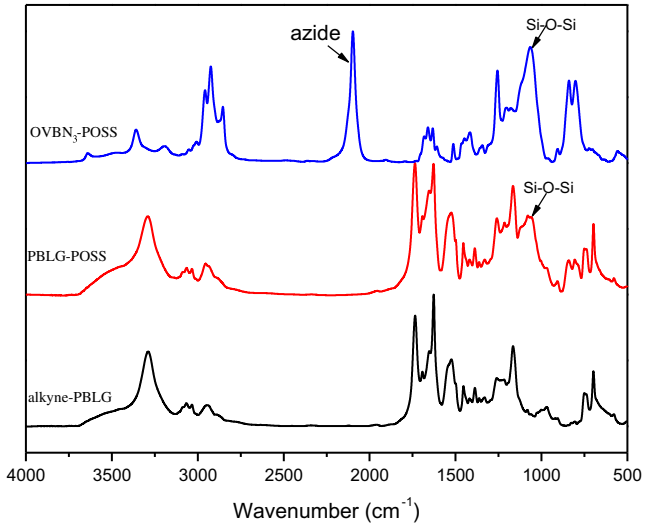

Fig. 4. FTIR spectra of (a) OVBN$_3$-POSS, (b) star PBLG$_4$-*b*-POSS, and (c) alkyne-PBLG$_4$.

3. Results and discussion

3.1. Synthesis of OVBN$_3$-POSS

The peaks for the vinyl group of VBC (ca. 5.3, 5.8, and 6.7 ppm) in Fig. 1(a) and Si–H protons (4.7 ppm) of $Q_8M_8^H$ in Fig. 1(b) disappeared in the spectrum of OVBC-POSS, supporting the complete reaction of hydrosilylation. The spectrum in Fig. 1(c) indicates that the vinyl groups of VBC underwent hydrosilylation of the Si–H bonds of $Q_8M_8^H$ in both the α and β configurations, i.e., a mixture of these two orientations exists. We observed the ratios of β to α linkages (1.64:1) for OVBC-POSS, according to the integration of the signals for the protons on the benzylic carbon atoms marked *b* (2H, β-side groups) and *b*′ (1H, α-side groups), benzyl CH_2 (**H**$_e$) at δ = 4.50 ppm, and the aromatic protons multiplet at 6.90–7.20 ppm, indicating the successful synthesis of OVBC-POSS. The complete substitution of chloride atoms by azido groups was confirmed by the ^{1}H NMR spectrum in Fig. 1(d). With the occurrence of the substitution reaction, the resonance of the benzyl CH_2 connected to the chloride atoms shifted to higher field – from 4.50 to 4.31 ppm. The observation that no remnant resonance existed at 4.50 ppm suggested that the substitution reaction occurred to completion under the reaction conditions. All other peaks assignment are summarized in Scheme 2(b) and (c).

3.2. Synthesis of alkyne-PBLG

Fig. 2(a) shows the ^{1}H NMR spectrum of BLG monomer in CDCl$_3$, the benzyloxycarbonyl ring protons resonated between 7.31 and 7.38 ppm, while the benzyl protons ($C_6H_5C\mathbf{H}_2-$) gave a doublet at 5.11 ppm. The singlet at 6.4 ppm was assigned to the proton on the ring nitrogen atom, with the other alkyl CH_2 protons coming upfield as multiplets between 2.0 and 2.6 ppm Fig. 2(b) shows the ^{1}H NMR spectrum of alkyne-PBLG in CDCl$_3$+15% TFA. The proton on the nitrogen atom of alkyne-PBLG resonated at singlet at 7.9 ppm, the singlet at 2.6 and 4.0 ppm corresponds to C≡C–H and C≡C–C$\mathbf{H}_2$, respectively, and the aromatic protons appeared as multiplets at 7.31–7.38 ppm. Molar masses of alkyne-PBLG were determined by ^{1}H NMR using the following equation:

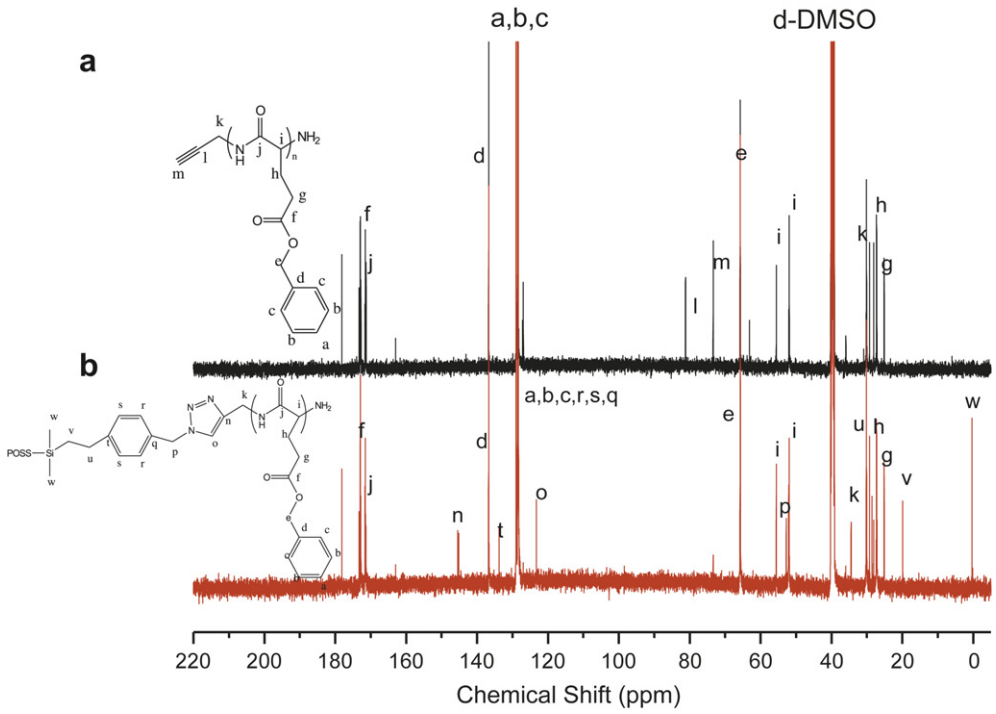

Fig. 5. ^{13}C NMR of (a) alkyne-PBLG$_4$, and (b) star PBLG$_4$-*b*-POSS in d-DMSO.

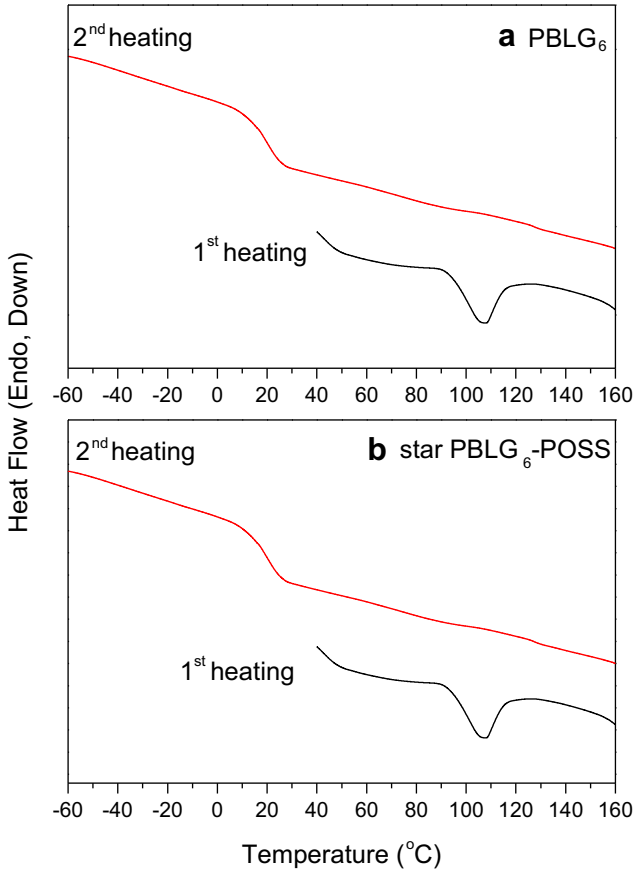

Fig. 6. DSC analyses of (a) alkyne-PBLG$_6$, and (b) star PBLG$_6$-*b*-POSS.

$$M_{n,\mathrm{PBLG}} = \frac{2I_b M_{\mathrm{BLG}}}{I_f} + M_{\mathrm{propargylamine}}$$

Where I_g and I_b are intensity of methylene protons ***b*** (alkyne-PBLG) from the PBLG main chain and methylene protons ***f*** of propargylamine initiator, respectively. $M_{\mathrm{propargylamine}}$ is the molar mass of propargylamine initiator. Table 1 lists the different molecular weight of the alkyne-PBLG by ^{1}H NMR.

3.3. Synthesis of star PBLG-*b*-POSS copolymers

Fig. 3 shows the ^{1}H NMR spectra of OVBN$_3$-POSS, alkyne-PBLG, and star PBLG-*b*-POSS. The peak assignments of alkyne-PBLG and OVBN$_3$-POSS have been shown in Figs. 1 and 2. In addition, the peaks of star PBLG-POSS is assigned in Scheme 2(d). The resonance of benzyl C**H**$_2$ of OVBN$_3$-POSS connected to the azide atoms significantly shifted to down field from 4.31 to 5.48 ppm of star PBLG-POSS. In addition, the methyl (C**H**$_3$) attached to silicone atom was found at 0.04 ppm from OVBN$_3$-POSS and the proton on the nitrogen atom from PBLG resonated at singlet at 7.9 ppm, also indicating the synthesis of star PBLG-*b*-POSS was successful. The complete disappearance of the characteristic azide and acetylene groups could be confirmed by FTIR analysis as shown in Fig. 4. The peak at 2100 cm^{-1}, corresponding to the azide absorbance to OVBN$_3$-POSS was totally disappeared in star PBLG-*b*-POSS and the Si—O—Si (siloxane) group absorption band of POSS, which appears at 1100 cm^{-1} in star PBLG—POSS copolymers, indicating that all the azide and acetylene functionalities participated in the click reaction.

The click reaction also can be characterized by ^{13}C NMR as shown in Fig. 5. Fig. 5(a) shows the carbonyl and amide carbon atom signals of alkyne-PBLG at 172.3 ppm and 171.4 ppm, respectively, while those at phenyl ring showed up at 136.4 ppm, with the other phenyl ring carbon atoms resonating around 128 ppm. The benzyl carbon (C$_6$H$_5$**C**H$_2$) and α-carbon (NHCO**C**) peaks came up at 66.0 ppm and 52.0 ppm (β-sheet conformation), respectively. A small peak at 55.1 ppm is come from the α-helix

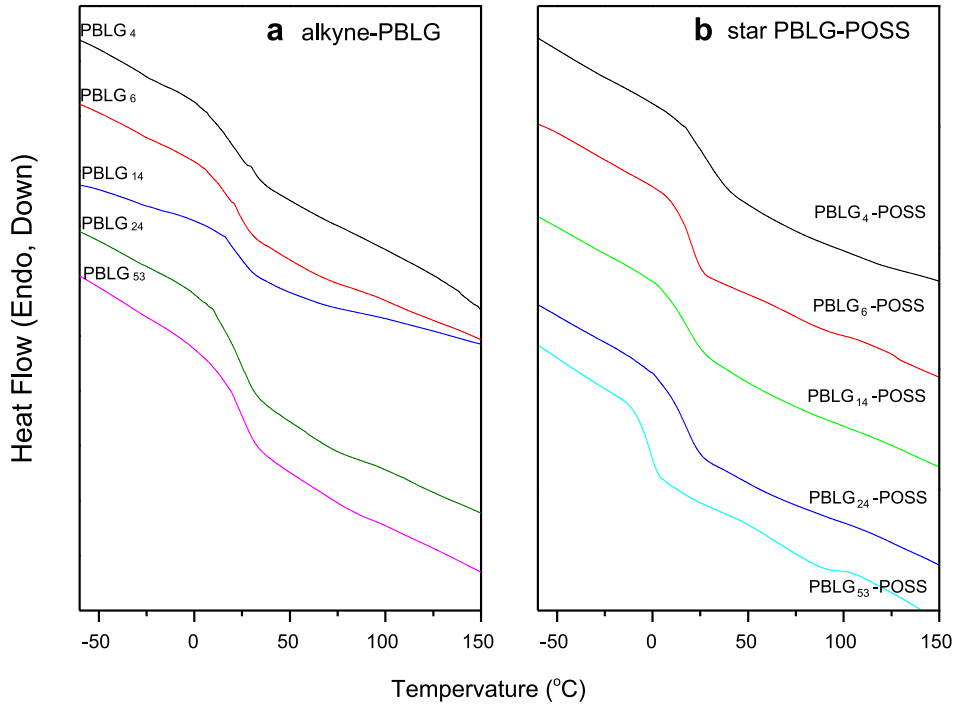

Fig. 7. DSC second heating run of (a) alkyne-PBLG, and (b) star PBLG-*b*-POSS.

conformation of α-carbon. The alkyne carbon signals of alkyne-PBLG were found at 81.0 ppm and 73.4 ppm. The remaining carbon signals for alkyne-PBLG are assigned in Fig. 5(a). Fig. 5(b) shows ^{13}C NMR of star PBLG-*b*-POSS. Clearly, the alkyne carbon signal at 81.0 ppm of alkyne-PBLG was disappeared in star PBLG-*b*-POSS. The peaks at 123.2 ppm and 145.3 ppm are the carbons of the triazole structures resulting from the click reaction. The methyl and methylene carbons of $OVBN_3$-POSS were remained in star PBLG-*b*-POSS at 0.2 ppm and 19.8 ppm, respectively. All other carbon signals for star PBLG-*b*-POSS are assigned in Fig. 5(b). All results based on ^{1}H NMR, ^{13}C NMR, and FTIR analyses indicated that the synthesis of star PBLG-*b*-POSS was successful.

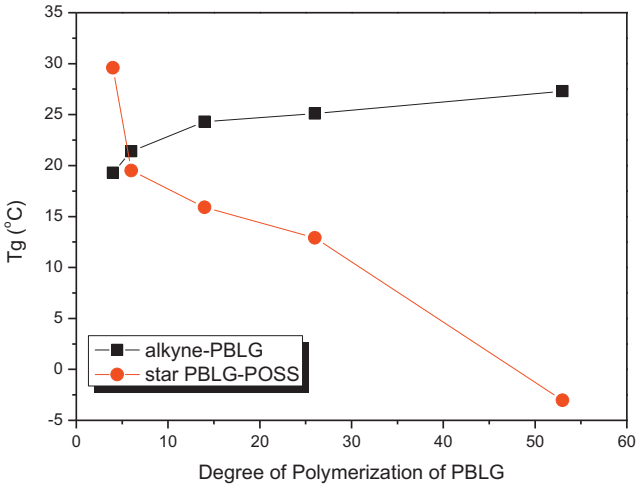

Fig. 8. T_g behavior with degree of polymerization for alkyne-PBLG and star PBLG-*b*-POSS.

3.4. Thermal analyses of star PBLG-*b*-POSS copolymers

Fig. 6 shows the DSC thermograms of alkyne-$PBLG_6$ and star $PBLG_6$-*b*-POSS. Both alkyne-$PBLG_6$ and star $PBLG_6$-*b*-POSS exhibits a nematic-like liquid crystal (LC) phase transition at ca. 106 °C during the first heating run, which was assigned to an irreversible change from a 7/2 to an 18/5 helical secondary structure [2]. The α-helix, which can be regarded as a rigid rod stabilized by intramolecular hydrogen bonding interaction, has its residues on a spiral pitch of ca. 0.54 nm, which is right-handed for L-α amino acids and has ca. 3.6 residues per turn, giving 18 residues in five turn. A second helical conformation is seven residues in two turns. The unusual (7/2) helices are transformed to the normal (18/5) helices via a broad first-order transition at ca. 106 °C. This transition is increased with the increase of degree of polymerization of PBLG as shown in Table 1. This transformation is irreversible as been by the absence in the second heating run. During the second heating run, we observed only one glass transition temperature (at ca. 20 °C) for the alkyne-$PBLG_6$ and star $PBLG_6$-*b*-POSS.

Fig. 7 shows the second heating run of all alkyne-PBLG and star PBLG-*b*-POSS samples. Clearly, the glass transition temperature of alkyne-PBLG is increased, with the increase of degree of polymerization [2]; however, on the contrary, the glass transition temperature of star PBLG-*b*-POSS is decreased with the increase of degree of polymerization. The molecular weight dependence of T_g behavior is shown in Fig. 8 and is reminiscent of the dependence found in other amorphous polymers such as the Fox–Flory equation:$T_g = T_g - K/M_n$. For alkyne-PBLG, the values of $T_g$and K are 27.0 °C and 31.8, respectively. However, the star PBLG-*b*-POSS shows an interesting case that the negative K values (−107) are about 3–4 times for linear PBLG, which is similar with previous study on polystyrene system by Danusso et al. due to the chemical dissimilarity end group effect and the increase of free volume in star polymers [35]. However, at the lowest molecular weight of $PBLG_4$, the T_g value of star $PBLG_4$-*b*-POSS is higher than linear alkyne-$PBLG_4$ ca. 10 °C which is probably due to the β-sheet

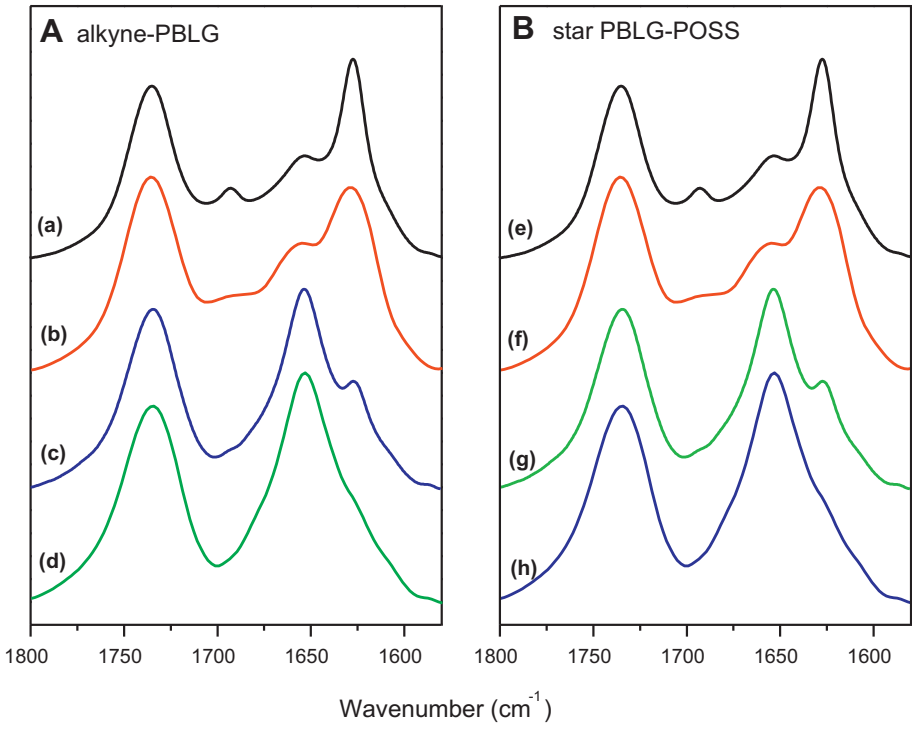

Fig. 9. FTIR spectra of (A) alkyne-PBLG for (a) $PBLG_4$, (b) $PBLG_6$, (c) $PBLG_{14}$, (d) $PBLG_{24}$, and (B) star PBLG–POSS for (e) $PBLG_4$–POSS, (f) $PBLG_6$–POSS, (g) $PBLG_{14}$–POSS, and (h) $PBLG_{24}$–POSS.

conformation of alkyne-$PBLG_4$ transformation to α-helix rigid rod like structure after incorporation of POSS unit in star $PBLG_4$-*b*-POSS system and the end group effect becomes unimportant at lower molecular weight of PBLG. The secondary structure transformation between alkyne-PBLG and star PBLG-*b*-POSS can be characterized by Fourier Transform Infrared spectroscopy (FTIR), solid state nuclear magnetic resonance (NMR), and wide-angle X-ray diffraction (WAXD) analyses in the following section.

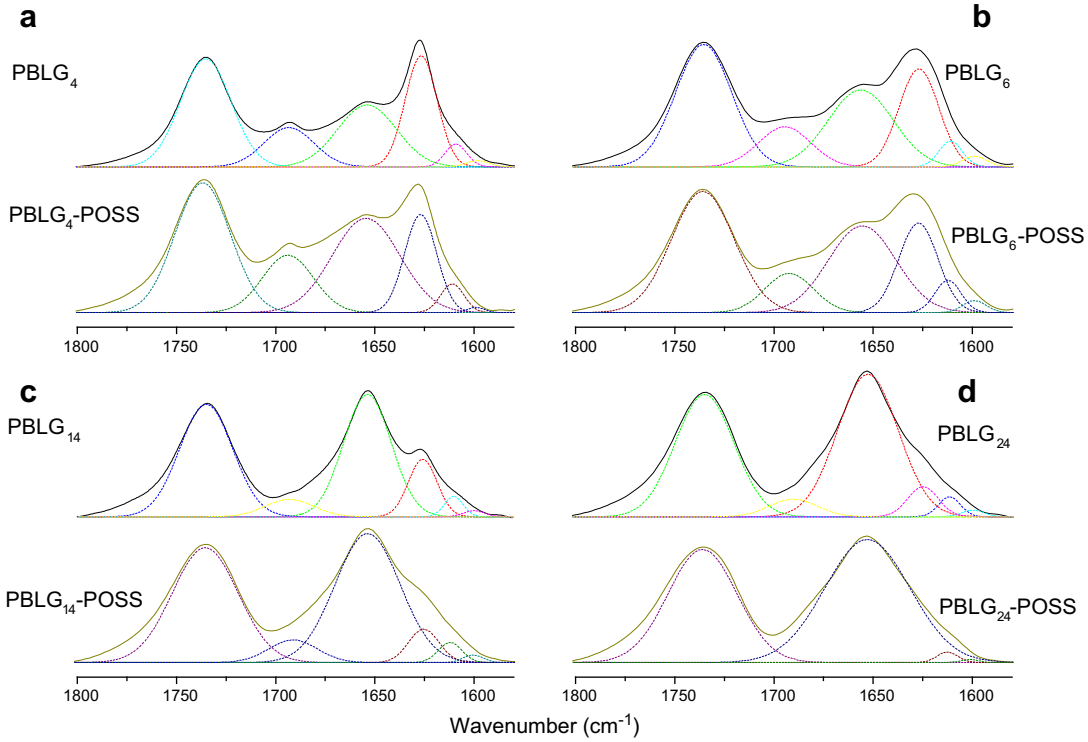

Fig. 10. Curve fitting results of (a) $PBLG_4$, (b) $PBLG_6$, (c) $PBLG_{14}$, and (d) $PBLG_{24}$, and their corresponding star PBLG-*b*-POSS.

Table 2
Curve fitting of secondary structure of alkyne-PBLG and star PBLG-*b*-POSS (υ: wavenumber (cm^{-1}), $W_{1/2}$: half-width (cm^{-1}), A_f: area fraction of each peak).

Samples	β-Sheet			α-Helix			Random coil		
	υ	$W_{1/2}$	A_f	υ	$W_{1/2}$	A_f	υ	$W_{1/2}$	A_f
$PBLG_4$	1693	30	21.4	1653	36	39.8	1627	19	38.6
$PBLG_4$–POSS	1693	30	21.6	1654	38	52.4	1627	19	25.8
$PBLG_6$	1694	30	18.9	1656	38	45.5	1627	21	35.6
$PBLG_6$–POSS	1693	30	16.9	1655	39	52.0	1627	21	31.1
$PBLG_{14}$	1693	29	10.1	1654	38	70.1	1626	17	19.8
$PBLG_{14}$–POSS	1692	28	10.4	1654	38	79.8	1625	18	9.8
$PBLG_{24}$	1690	28	8.1	1653	36	83.1	1625	18	8.8
$PBLG_{24}$–POSS	–	–	0	1652	50	100	–	–	0
$PBLG_{53}$	–	–	0	1652	50	100	–	–	0
$PBLG_{53}$–POSS	–	–	0	1652	50	100	–	–	0

3.5. Conformation study of the peptide segment

FTIR studies at room temperature were performed to obtain information about the conformation of the peptide segment of the alkyne-PBLG and star PBLG-*b*-POSS as shown in Fig. 9. These spectra were first analyzed by the second derivative technique [9], indicating that the amide I band at 1655 cm^{-1} is characteristic for the α-helical secondary structure. For polypeptides possessing a β-sheet conformation, the position of the amide I band shifted to 1627 cm^{-1}, where random coil or turn population is located at 1693 cm^{-1}, free carbonyl of side chain group of PBLG is at 1734 cm^{-1}, and the peaks at 1607 cm^{-1} and 1594 cm^{-1} are corresponding to the benzene stretching of side chain group of PBLG. The second step was used the deconvolution technique in a series of Gaussian distributions to quantify the fraction of each of the peaks as shown in Fig. 10. Table 2 summarizes the curve fitting results of amide I group for β-sheet; α-helical and random coil structures. Clearly, the fraction of α-helical secondary structure was increased with the increase of degree of polymerization in both alkyne-PBLG and star PBLG-*b*-POSS system, which is similar with the report by Papadopoulos et al. [2]. The low degree of polymerization (DP < 18), both secondary structures are present, but as the degree of polymerization increases, the α-helical secondary structure is favored. In addition, all star PBLG-*b*-POSS after click reaction has higher fraction of α-helical secondary structure than their corresponding alkyne PBLG with same degree of polymerization of polypeptide.

The secondary structures of PBLG also can be identified on the basis of the distinctly different resonances observed in their solid state NMR spectra. The ^{13}C CP/MAS spectra of alkyne-PBLG and star PBLG-*b*-POSS at room temperature are shown in Fig. 11. The peaks assignments are similar with Fig. 5, but broad band in solid state NMR was observed due to the dipole–dipole interaction and chemical shift anisotropy [36]. In star PBLG-*b*-POSS, the methyl carbon attached to silicone atom was found at 5.0 ppm, also indicating the synthesis of star PBLG-*b*-POSS was successful. The different ^{13}C chemical shift of the C_α and amide C=O resonances are attributed to the local conformations of individual amino acid residues characterized by the dihedral angles and the type of intermolecular and intramolecualr hydrogen bonding interactions [37]. In the case of PBLG, the longer side chains can stabilize α-helical secondary structure and correspondingly, the chemical shift of the C_α and amide C=O resonances at 57.5 and 176 ppm. In the β-sheet conformation, these chemical shifts are displayed upfield by ca. 4–5 ppm relative to the α-helical values at 52.7 and 172 ppm. Since the amide C=O resonance in the β-sheet conformation partially overlaps with the signal from the side-chain ester, the distinction of the peptide secondary structure is best from the distinctly different Cα resonances (δ = 57.5 ppm and δ = 52.7 ppm for α-helices and β-sheets, respectively) [2]. Clearly, the peptide secondary structure is

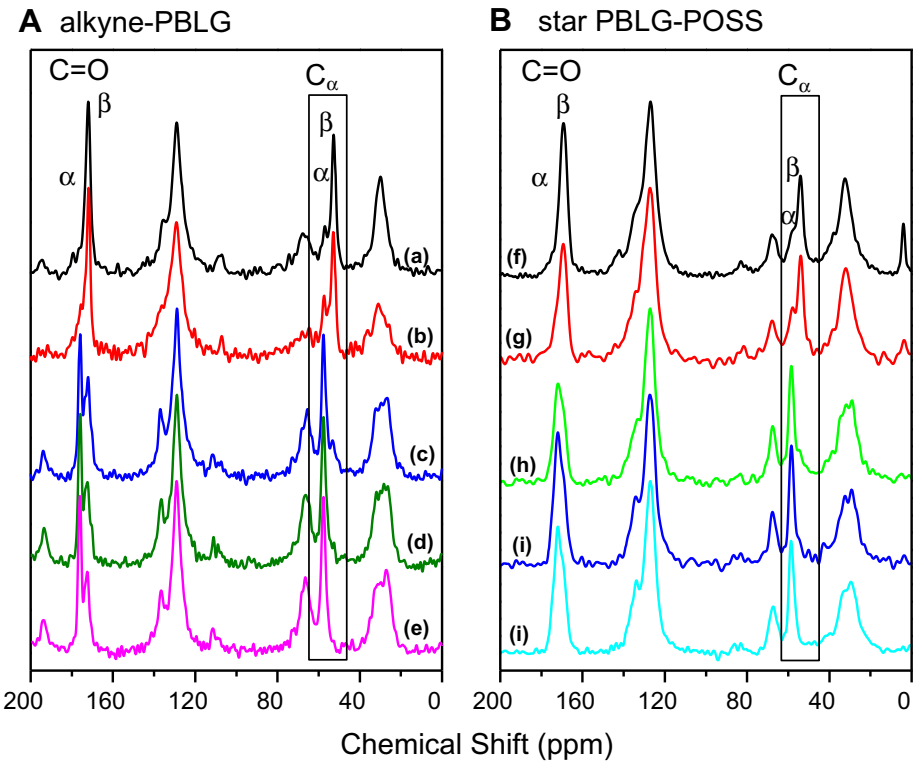

Fig. 11. ^{13}C solid state NMR spectra of (A) alkyne-PBLG for (a) $PBLG_4$, (b) $PBLG_6$, (c) $PBLG_{14}$, (d) $PBLG_{24}$, (e) $PBLG_{53}$ and (B) star PBLG-*b*-POSS for (f) $PBLG_4$–POSS, (g) $PBLG_6$–POSS, (h) $PBLG_{14}$–POSS, (i) $PBLG_{24}$–POSS, (j) $PBLG_{53}$–POSS.

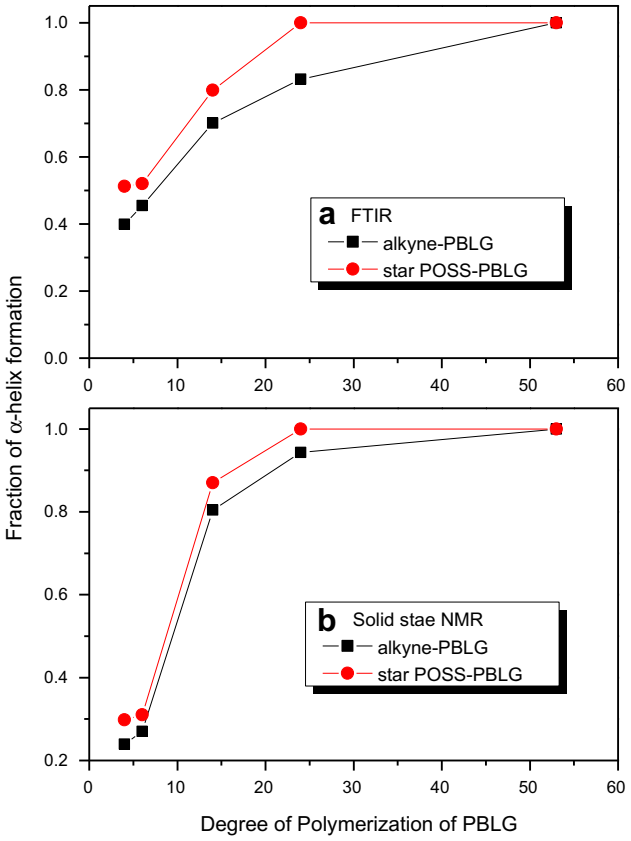

Fig. 12. Fraction of α-helix formation with degree of polymerization for alkyne-PBLG and star PBLG-*b*-POSS by (a) FTIR, and (b) solid state NMR analyses.

predominantly α-helical when the degree of polymerization of PBLG is 24 and 53 for both alkyne-PBLG and star PBLG-*b*-POSS, whereas β-sheets are formed when PBLG is very short ($PBLG_4$ or $PBLG_6$), which is similar with FTIR study. The fraction of secondary structure also can be analyzed by deconvolution technique in a series of Gaussian distributions to quantify the fraction of each of the peaks ($\delta = 57.5$ ppm for α-helices and $\delta = 52.7$ ppm for β-sheets). Fig. 12 compares the fractions of α-helix formation that are obtained by FTIR and solid state NMR analyses. We need to emphasize that the values from FTIR and solid state NMR should be different [38,39], but the trend of fraction of α-helical secondary structure change is similar, where the fraction of α-helical secondary structure was increased with the increase of degree of polymerization in both alkyne-PBLG and star PBLG-*b*-POSS system, and all star PBLG-*b*-POSS after click reaction has higher fraction of α-helical secondary structure than their corresponding alkyne PBLG with same degree of polymerization of polypeptide.

The similar phenomena also can be characterized from wide-angle X-ray diffraction at 393 K to identify the secondary structure change of alkyne-PBLG and star PBLG-*b*-POSS as shown in Fig. 13. The effects of chain length and after incorporation of POSS in PBLG on the type of secondary structure are discussed. For alkyne-PBLG as shown in Fig. 13(a), the diffraction pattern of PBLG at degree of polymerization (DP = 14) shows the presence of two secondary structures. For first peak at $2\theta = 4.57°$ reflects the distance ($d = 1.67$ nm) between backbones in the antiparallel β-pleated sheet structure and the reflection at 16.2° ($d = 4.7$ nm) represents the intermolecular distance between adjacent peptide chains with one lamellae. The three reflections at higher angles, with relative position $1:3^{1/2}:4^{1/2}$, relative to the primary peak at q^*, are indexed

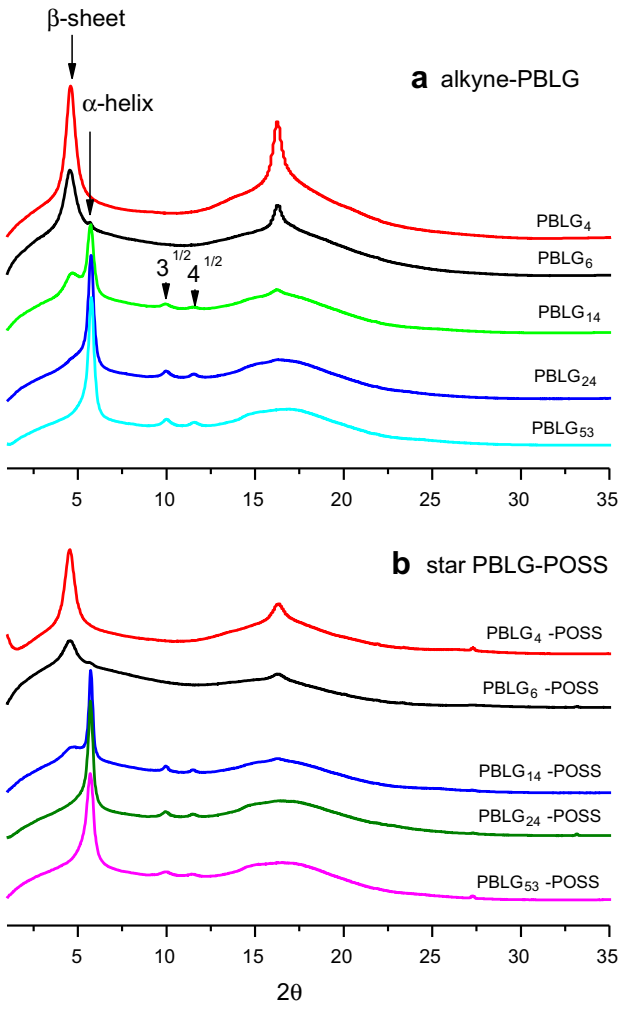

Fig. 13. WAXD of (a) alkyne-PBLG and (b) star PBLG-*b*-POSS with different degree of polymerization at 393 K.

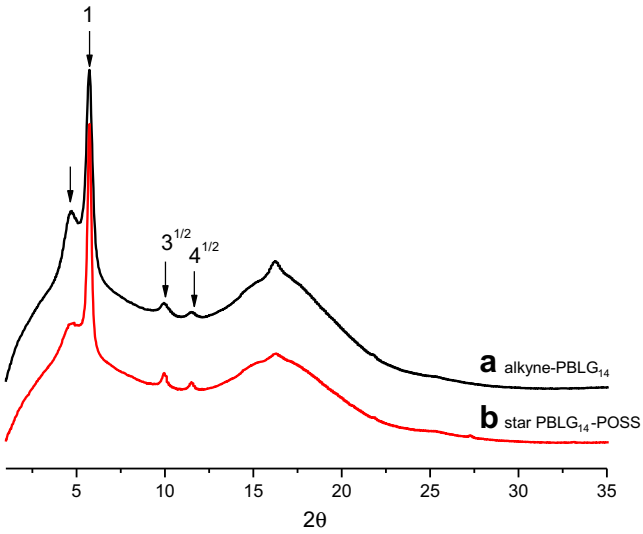

Fig. 14. WAXD analyses of (a) alkyne-$PBLG_{14}$ and (b) star $PBLG_{14}$-*b*-POSS.

according to the (10), (11), and (20) reflections of a 2D hexagonal packing of cylinders composed of 18/5 α-helices with a cylinder distance of 1.36 nm [2]. The structure of PBLG has been described as a nematic-like para crystal with a periodic packing of α-helices in the direction lateral to the chain axis. The broad amorphous at ca. 16° originates at mainly from the long amorphous side chain. Further increase the degree of polymerization of PBLG (DP = 24, and 53), the diffraction peaks at 4.57° associated with the β-sheet secondary structure is absent, suggesting the absence of that particular conformation from the longer peptides. In addition, the α-helical conformations are better packed in the longer peptide. Decreasing the length of the PBLG chain (DP = 4, and 6) leads to a destabilization of the α-helical secondary structure and the β-sheet secondary structure was observed at $2\theta = 4.57°$ and 16°. These results are agreement with the FTIR and solid state NMR analyses. On the basis of the results from the FTIR, NMR, and WAXD investigation, we obtain the information for the alkyne-PBLG: for low degree of polymerization (DP < 18), both secondary structures are present, but as the degree of polymerization increases, the α-helical secondary structure is favored.

The WAXD patterns of the star PBLG-*b*-POSS recorded at 393 K are presented in Fig. 13(b). For the star PBLG-*b*-POSS with the longer PBLG segments (DP > 24), only one set of Bragg peaks at diffraction angles with a ratio of $1:3^{1/2}:4^{1/2}$ is observed, indicating a columnar hexagonal arrangement of the molecules. Upon decreasing the length of the peptide segment (DP < 14) of star PBLG-*b*-POSS, a considerable fraction of the peptide segments has a β-sheet secondary structure, which is similar to those obtained for the corresponding alkyne-PBLG. Fig. 14 summarizes the WAXD patterns of alkyne-$PBLG_{14}$ and star $PBLG_{14}$-*b*-POSS. Clearly, the star $PBLG_{14}$-*b*-POSS after click reaction has higher fraction of α-helical secondary structure than their corresponding alkyne-$PBLG_{14}$. As a result, the incorporation of the POSS moiety at the PBLG chain end leads to intramolecular hydrogen bonding between the POSS and PBLG units that enhances the formation of the PBLG α-helix; recall that this conformation is stabilized through such interactions, which has been confirmed in our previous study by 2D-FTIR spectroscopy [20]. From this information, it can be explained that even if peptides partly adopt the α-helical and β-sheet conformation when anchored to POSS as a star polymer, conformational stabilization occurs, most of the peptide segments are constrained in the α-helical secondary structure. In addition, the intrinsic compatibility of star polypeptides makes them suitable candidates for compatibilizer in mixture of linear polypeptide chains [30].

4. Conclusions

The well-defined star PBLG-*b*-POSS copolymers through the combination of the ring-opening polymerization of Glu–NCA are followed by the click reaction in the presence of multifunctional azide-POSS. As the PBLG blocks are attached to the POSS nanoparticle, the fraction of α-helical secondary structure is increased due to the intramolecualr hydrogen bonding interaction between POSS and PBLG. Star PBLG-*b*-POSS exhibit more conformation stability than the linear PBLG, indicating that containing molecular architecture of the PBLG causes a change in the liquid crystal ordering and alignments.

Acknowledgments

This work was supported financially by the National Science Council, Taiwan, Republic of China, under Contract No. NSC 97-2221-E-110-013-MY3 and NSC 97-2120-M-009-003. The WAXD experiments were conducted at beamline BL17B3 at the National Synchrotron Radiation Research Center (NSRRC), Taiwan.

References

[1] Klok HA, Lecommandoux S. Adv Mater 2001;13:1217.
[2] Papadopoulous P, Floudas G, Klok HA, Schnell I, Pakula T. Biomacromolecules 2004;5:81.
[3] Flory PJ. Proc R Soc London Ser A 1956;234:73.
[4] Robinson C, Ward JC. Nature 1957;180:1183.
[5] Yu SM, Conticello VP, Zhang G, Kayser C, Fournier MJ, Mason TL, et al. Nature 1997;389:167.
[6] Tohyama K, Miller WG. Nature 1981;289:813.
[7] Kuo SW, Lee HF, Chang FC. J Polym Sci Part A Polym Chem 2008;46:3108.
[8] Gitsas A, Floudas G, Mondeshki M, Spiess HW, Aliferis T, Iatrou H, et al. Macromolecules 2008;41:8072.
[9] Sanchez-Ferrer A, Mezzenga R. Macromolecules 2010;43:1093.
[10] Zhou QH, Zheng JK, Shen ZH, Fan XH, Chen XF, Zhou QF. Macromolecules 2010;43:5637.
[11] Lee HF, Sheu HS, Jeng US, Huang CF, Chang FC. Macromolecules 2005;38:6551.
[12] Papadopoulos P, Floudas G, Schnell I, Aliferis T, Iatrou H, Hadjichristidis N. Biomacromolecules 2005;6:2352.
[13] Rao J, Zhang Y, Zhang J, Liu S. Biomacromolecules 2008;9:2586.
[14] Ibarboure E, Papon E, Rodriguez-Hernandez J. Polymer 2007;48:3717.
[15] Ibarboure E, Rodriguez-Hernandez J. J Polym Sci Part A Polym Chem 2006;44:4668.
[16] Klok HA, Langenwalter JF, Lecommandoux S. Macromolecules 2000;33:7819.
[17] Lecommandoux S, Achard MF, Langenwalter JF, Klok HA. Macromolecules 2001;34:9100.
[18] Crespo JS, Lecommandoux S, Borsali R, Klok HA, Soldi V. Macromolecules 2003;36:1253.
[19] Papadopoulos P, Floudas G, Schnell I, Lieberwirth I, Nguyen TQ, Klok HA. Biomacromolecules 2006;7:618.
[20] Kuo SW, Lee HF, Huang WJ, Jeong KU, Chang FC. Macromolecules 2009;42:1619.
[21] Xu H, Kuo SW, Lee JS, Chang FC. Macromolecules 2002;35:8788.
[22] Li GZ, Wang LC, Ni HL, Pittman CU. J Inorg Organometal Polym 2001;11:123.
[23] Mark JE. Acc Chem Res 2004;37:946.
[24] Pielichowaski K, Niuguna J, Janowski B, Pielichowski J. Adv Polym Sci 2006;201:225.
[25] Kuo SW, Wu YC, Lu CH, Chang FC. J Polym Sci Part B Polym Phys 2009;47:811.
[26] Huang KW, Tsai LW, Kuo SW. Polymer 2009;50:4876.
[27] Lu CH, Kuo SW, Chang FC. Macromol Rapid Commun 2009;30:2121.
[28] Lu CH, Kuo SW, Huang CF, Chang FC. J Phys Chem C 2009;113:3517.
[29] Yen YJ, Kuo SW, Huang CF, Chen JK, Chang FC. J Phys Chem B 2008;112:10821.
[30] Gitas A, Floudas G, Mondeshki M, Butt HJ, Spiess HW, Iatrou H, et al. Biomacromolecules 2008;9:1959.
[31] Abraham S, Ha CS, Kim IL. J Polym Sci Part A Polym Chem 2006;44:2774.
[32] Daly WH, Poche D. Tetrahedron Lett 1988;29:5859.
[33] Wu IC, Kuo SW. Polymer 2010;51:3948.
[34] Agut W, Taton D, Lecommandoux S. Macromolecules 2007;40:5653.
[35] Danusso F, Levi M, Gianotti G, Turri S. Polymer 1993;34:3687.
[36] Randall JC. ACS symposium series, NMR and macromolecules: sequence, dynamic, and domain structure. Washington, D.C: American Chemical Society; 1984.
[37] Murata K, Katoh E, Kuroki S, Ando I. J Mol Struct 2004;689:223.
[38 Huang MW, Kuo SW, Wu HD, Chang FC, Fang SY. Polymer 2002;43:2479.
[39] Hill DJT, Whittaker AK, Wong KW. Macromolecules 1999;32:5285.